Revision 1

The crystal structures of $Mg_2Fe_2C_4O_{13}$, with tetrahedrally coordinated carbon, and $Fe_{13}O_{19}$, synthesized at deep mantle conditions.

Authors: Marco Merlini[1], Michael Hanfland[2], Ashkan Salamat[3], Sylvain Petitgirard[4], Harald Müller[2]

Affiliations:

[1]Dipartimento di Scienze della Terra, Università degli Studi di Milano, Via Botticelli 23, 20133 Milano (Italy).

[2]ESRF - The European Synchrotron Radiation Facility, 71, avenue des Martyrs, 38000 Grenoble, France

[3]Lyman Laboratory of Physics, Harvard University, Cambridge, MA 02138, USA

[4]Bayerisches Geoinstitut, Universität Bayreuth, 95440, Germany.

Corresponding author:

Marco Merlini

Dipartimento di Scienze della Terra,

Università degli Studi di Milano,

via Botticelli, 23

I-20133 Milano (Italy)

Tel. +39 02 50315622

E-mail: marco.merlini@unimi.it

Abstract

Within the Earth's rich mineral diversity, and specifically in the lower mantle, magnesite, $MgCO_3$, is considered the most important carbonate. It is understood that the presence of iron can significantly modify the phase stability of carbonates, and at lower mantle conditions complex red-ox reactions can occur. A significant challenge has been to develop methods to determine these ultra-deep redox equilibria as well as knowledge of candidate minerals for carbon storage in order to assess the Earth's deep carbon cycle. However, until now, the exact structural description of the phases involved and quantitative chemical reaction descriptions have remained elusive. We simulated the redox decomposition of magnesium-siderite at pressures and temperatures corresponding to the top of the Earth's D'' layer (135 GPa and 2650 K). It transforms into new phases, with unexpected stoichiometry. We report their crystal structure, based on single-crystal synchrotron radiation diffraction on a multi-grain sample, using a charge-flipping algorithm. $Mg_2Fe_2(C_4O_{13})$ is monoclinic, a = 9.822(3), b = 3.9023(13), c = 13.154(5) Å, β = 108.02(3)°, V = 479.4(3) Å^3 (at 135 GPa). It contains tetrahedrally coordinated carbon units, corner-shared in truncated C_4O_{13} chains. Half of the cations, are divalent, and half trivalent. The carbonate coexists with a new iron oxide, $Fe_{13}O_{19}$, monoclinic, a = 19.233(2), b = 2.5820(13), c = 9.550(11) Å, β = 118.39(3)°, V = 417.2(5) Å^3 (at 135 GPa). It has a stoichiometry between hematite, Fe_2O_3, and magnetite, Fe_3O_4. The formation of these unquenchable phases indicates, indirectly, the formation of reduced-carbon species, possibly diamond. These structures suggest the ideas that the mineralogy of the lower mantle and D'' region may be more complex than previously estimated. This is especially significant concerning accessory phases of fundamental geochemical significance and their role in ultra-deep iron-carbon redox coupling processes, as well as the iron-oxygen system, which certainly play an important role in the lower mantle mineral phase equilibria.

Keywords

Carbonate, tetrahedrally coordinated carbon, iron oxide, high pressure, single crystal diffraction

Introduction

Carbonates are important minerals in the Earth's mantle, as revealed by diamond inclusion studies (Berg 1986) and high-pressure experiments (Rohrbach and Schmidt 2011). At the Earth's crust-atmosphere-hydrosphere interface, calcium-rich carbonates are the main carbon repository phases. Magnesite, $MgCO_3$, is considered an important candidate for the main carbonates in the lower mantle, and it remains stable in the calcite-type structure up to 80 GPa and several thousand Kelvin. Above these conditions, it transforms to a high-pressure polymorph (Isshiki et al. 2004; Boulard et al. 2011), with a predicted complex structure (Oganov et al. 2008, 2013) based on tetrahedrally coordinated carbon (Arapan et al. 2007). These features have been eventually confirmed by X-ray powder diffraction patterns experiments at 82 GPa and 2350 K and spectroscopic analysis on quenched materials (Boulard et al. 2011), even if no structure determination was achieved. The presence of Fe can significantly modify the phase stability of carbonates (Rohrbach and Schmidt 2011, Boulard et al. 2011,2012). The end-member siderite, $FeCO_3$, in particular, decomposes into Fe_3O_4 magnetite and CO-fluid at low pressures and high temperatures (Tao et al. 2013). Above a few GPa of pressure it is stable up to the melting line, but at much higher pressures and temperatures a disproportionation reaction is observed. The discovery of these new phases with unexpected stoichiometry, e.g. $Fe_4(CO_4)_3$ (Boulard et al. 2012), suggests that the equilibria of carbonates cannot be fully understood only in terms of the very well-known low-pressure phases. Crucially, the $Fe_4(CO_4)_3$ formula indicates that Fe should be entirely trivalent, a feature unknown in the crystal chemistry of the common low-pressure carbonates. Studying the physical and chemical behavior of iron-carbonates in the Earth's mantle is therefore fundamental to our understanding of the geochemistry of carbon. This has been elegantly demonstrated (Rohrbach and Schmidt 2011) using red-ox reactions to explain diamond stability and carbonatitic magmas. In considering the high-pressure disproportionation of pure siderite into a mixture of $Fe_4(CO_4)_3$, Fe_3O_4, and diamond, the behavior of carbonates with stoichiometry intermediate between magnesite and siderite is still unknown. This is concerning especially when trying to build a sensible model of the lower mantle and is a fundamental issue that must be clarified e.g. magnesite in the lower mantle could shift towards the siderite component, especially in the D'' layer at the base of the lower mantle, where enrichment of Fe may occur, because of reaction with outer-core material (Knittle and Jeanloz 1991; Otsuka and Karato 2012). However, pure siderite in the mantle is unlikely. Here, we studied the stability of Mg-siderite samples at D'' layer conditions. We applied a cutting-edge synchrotron X-ray, single-crystal diffraction technique (Merlini and Hanfland 2013) to monitor structural changes at high pressure and high temperature.

Materials and methods

Natural siderite samples taken from Puits de Villaret (La Mure, France) were used for the experiment. Elemental analysis confirmed a Mg-siderite composition, with trace amounts of Ca and Mn. The crystal chemistry formula is $Fe_{0.70}Mg_{0.26}Mn_{0.025}Ca_{0.015}(CO_3)$, simplified into $Fe_{0.7}Mg_{0.3}(CO_3)$ throughout the manuscript. The Fe content in the sample permitted the investigation of a mixed Mg-Fe sample and assured enough Fe for laser radiation absorption at ~1.25 eV, essential for homogeneous single-crystal high-temperature annealing (Salamat et al. 2014). High-pressure experiments were performed at the ID09A beamline at the ESRF synchrotron facility (Grenoble, France). A full description of the beamline setup has been reported (Merlini and Hanfland 2013). We used a monochromatic beam ($\lambda = 0.414314$ Å) with beam size 15×15 μm^2 on the sample. The detector used was a Mar555 flat panel. A crystal of $15 \times 15 \times 5$ μm^3 was placed in the high-pressure chamber of a membrane-type DAC, equipped with Boheler-Almax-designed diamonds, beveled with a lower section of 150 μm diameter. We used a rhenium gasket, preindented to a thickess of 30 μm. The sample chamber was loaded with Ne, which acted as pressure-transmitting medium, pressure marker (Fei et al. 2007) and insulating material for high-temperature heating. We also monitored the pressure by measuring the fluorescence line of a Sm-doped Sr-borate (Datchi et al., 1997). We performed single-crystal data collections by ω-step scan rotation, with 1° step, in the angular range -30/+30°. Normally, we performed two data collections at different χ angles (Busing and Levy, 1967): $\chi = 0$ and $\chi = 90°$, in order to collect all the diffraction peaks in the accessible reciprocal space, determined by the DAC opening cone. Diffraction data were handled using the Crysalis software (Oxford Diffraction, 2008), with instrumental geometrical parameters (sample-to-detector distance, detector tilt) previously refined against a standard quartz single crystal. The integrated single-crystal data were processed with Jana2006 and Superflip software (Petricek et al. 2014; Palatinus and Chapuis 2007). In-situ double-sided laser heating was performed at ID27 of the ESRF using two Nd-doped Y-Al-garnet lasers. Temperature determination was carried out using pyrometry on the collected black body emission using Schwarzschild optics (Petitgirard et al. 2014).

Results: disproportionation of (Fe,Mg)CO_3

The single crystal of Mg-siderite was compressed up to 135 GPa at ambient temperature, and structure refinements confirmed its low-pressure rhombohedral symmetry (see also Deposit Items). After a first attempt at annealing at 1800 K and 135 GPa, no structural changes were observed. A second annealing was performed at a higher temperature of 2650 K. During the annealing the pressure increased to 141 GPa. Immediately, we observed that the sample was no longer transparent, indicating the occurrence of a transformation. This was confirmed by the presence of new diffraction spots. The number of Bragg peaks is consistent with the presence of multiple single crystal domains, belonging to one or more phases; we observed that these peaks were sharp and with minimum overlap. Single-crystal diffraction data was collected with the conventional procedure for this technique, using a large X-ray beam to irradiate all of the single crystal. With the help of a 3D reciprocal space visualizer, we manually selected the diffraction features belonging to four single-crystal domains, and we were able to index all of them successfully. These resulted in two C-centered monoclinic lattices: a=9.822(3), b=3.9023(13), c=13.154(5) Å, β=108.02(3)°, V=479.4(3) Å^3 and the other two in a different C-centred monoclinic cell: a=19.233(2), b=2.5820(13), c=9.550(11) Å, β=118.39(3)°, V=417.2(5) Å^3. There is no apparent geometrical relationship between the two different unit cells. This suggests that the original single crystal decomposed with multiple nucleations of the new phases. Step scans during data collection were performed, with the diamond anvil cell in two different orientations to permit the collection of diffraction data from all of the available reciprocal space. The integrated Bragg peak intensities for the two sets of crystals were merged to have enough data for carrying out structure solutions. A successful structure solution was achieved for both phases, using a combined charge-flipping algorithm approach and difference Fourier analysis. The charge-flipping algorithm (Oszlanyi and Suto 2004) does not require a-priori knowledge of the chemical formula and symmetry, and we take great advantage of this feature, since the presence of the two different type of lattices suggests a disproportionation reaction, with unknown chemical formula for the new phases, different from the starting carbonate. Using this powerful method we were able to determine the structures of a novel carbonate and an iron oxide. Furthermore, crystal structure refinements were achieved for both carbonate (Table 1) and iron-oxide (Table 2) phases. Precise atomic position and site occupancy determinations also provide the stoichiometry and fine structural details for these new phases (see also Deposit Items).

$Mg_2Fe_2(C_4O_{13})$

The nominal stoichiometry for the high pressure carbonate is $Mg_2Fe_2(C_4O_{13})$. The unconstrained refinement of Mg and Fe occupancy indicates a composition richer in Fe than nominal stoichiometry, and a lower Fe/Mg ratio than the original Mg-siderite. The structure is based on the presence of truncated tetrahedral chains C_4O_{13}, with Mg and Fe cations chemically bonded to the oxygen atoms of these chains, with no other free anions (Fig. 1). The experimental C–O distances in the carbon tetrahedra are in the range 1.25–1.35 Å, in strong agreement with predicted values (Oganov et al. 2008, 2013). The two larger cation sites are present in the structure, featuring distorted irregular [7] and [9]-fold coordination geometry. The refinement of the site occupancy indicates a disordered distribution of Mg and Fe in both sites. For stoichiometric and vacancy-free

$Mg_2Fe_2(C_4O_{13})$, all the Fe atoms are trivalent. For the actual $Mg_{1.6}Fe_{2.4}(C_4O_{13})$, a mixed 3+/2+ valence state must be assumed, with a high Fe^{3+}/Fe^{2+} ratio. Single-crystal diffraction data were also collected on decompression, and they provided volume measurements for the pressure interval of 141–40 GPa. These data are fitted with a 3rd-order Birch Murnagham equation of state (Deposit Items), and the extrapolation to ambient pressure indicates a bulk modulus $K_0 = 173(8)$ GPa and density $\rho_0 = 3.92(1)$ g/cm^3. We observe that $Mg_2Fe_2(C_4O_{13})$ is isostructural to synthetic $Ba_2Gd_2(Si_4O_{13})$ silicate (Wierzbicka-Wieczorek et al. 2010).

$Fe_{13}O_{19}$

The iron-oxide structure coexisting with the high-pressure $Mg_2Fe_2(C_4O_{13})$ carbonate was determined using a similar approach. The stoichiometry derived from the structure solution is $Fe_{13}O_{19}$, therefore with one divalent and twelve trivalent iron atoms per formula units. $Fe_{13}O_{19}$ possesses a new structure type, and its topology is not reported in compounds with comparable stoichiometry. Crystal structure and site occupancy refinements indicate a full Fe occupancy in all the cation sites. The $A^{2+}B^{3+}{}_{12}O_{19}$ stoichiometry is also common in a class of semiconductor materials (Pullar 2012). $Fe_{13}O_{19}$ is intermediate in composition between hematite Fe_2O_3 and magnetite Fe_3O_4, and close to the hematite end-member. The structure (Fig. 2) is almost a single layer structure, with the *b* lattice parameter corresponding to the length of an O-O octahedral edge. In the structure, there are two non-equivalent octahedral sites, formed by edge sharing one single and one double octahedral chains. These chains are connected in the structure by five large Fe-centered, [7] and [8] coordinated polyhedra. The low agreement factors from the structure refinements (Table 2 and Deposit Items) and sensible ADP's (atomic displacement parameters) values assess the accuracy of its determination. The interatomic distances in the octahedral sites may indicate low spin state cf. reference literature data (Fig. 3) (Shannon 1976; Lavina et al. 2012; Merlini et al. 2012). Decompression data provide experimental volumes for equation of state determination, resulting in a bulk modulus K_0 = 202(4) GPa and ambient-pressure density ρ_0=5.78(2) g/cm^3, as derived with a third-order BM EoS fit (Deposit Items).

Discussion

The single crystal of Mg-siderite underwent a disproportionation reaction at high pressures and temperatures into an assemblage of Fe^{3+}-bearing carbonate, Fe^{3+} oxide, and a reduced phase. We observed at least four different crystals, indicating a multiple nucleation of the newly formed phases. We could not recover the sample after decompression, since it broke down below 40 GPa, and the very small fragments were dispersed as soon as the diamond anvil cell was opened and Ne, gas, flowed out. From the decompression data these newly observed phases appear to be metastable and, as yet, unquenchable. One possible explanation is that during the pressure release, the low electronic spin Fe transforms back into a high-spin state, resulting in a large volume change and consequent rupture on the interface of the grain boundary. Diamond formation should have been observed, similarly to TEM analysis on samples recovered in lower-pressure experiments (Boulard et al. 2011, 2012). Starting from the measured Mg-siderite composition, we can balance the disproportionation reaction fixing the starting carbonate and pure $Fe_{13}O_{19}$ formulas :

$$93\ Fe_{0.7}Mg_{0.3}CO_3 = 20\ Mg_{1.395}Fe_{2.605}(C_4O_{13}) + Fe_{13}O_{19} + 13\ C$$

It is noted that the computed Fe/Mg ratio in high-pressure carbonate is in close agreement with site occupancy refined from the X-ray single-crystal data (Deposit Items). The experimental conditions and the annealing temperature are comparable to the pressures of the Earth's D'' layer and match the lower estimations of the geotherm at these pressures (Anderson 1982). The instability of the rhombohedral $(Mg,Fe)CO_3$ carbonate, is therefore confirmed for lowermost mantle conditions. The structural and chemical behavior of carbonate minerals appear to be very complex, being especially dependent on the Fe content in the $(Mg,Fe)CO_3$ solid solution. Pure magnesite very likely undergoes a polymorphic isochemical transition, structure based on polymerized CO_4 group (Isshiki et al. 2004; Oganov et al. 2008, 2013; Arapan et al. 2007). Our experimental data indicate new stoichiometry for mixed (Mg,Fe) carbonates decomposition products, with trivalent iron in a high-pressure carbonate phase. This feature requires additional anionic groups in the structure, and in $Mg_2Fe_2(C_4O_{13})$ this is achieved with the truncation of polymeric chains, resulting in one additional apical oxygen available for chemical bonds with Mg and Fe cations. This feature is an intermediate to the observed $Fe_4(CO_4)_3$ stoichiometry in the pure iron carbonate system (Boulard et al. 2012).

Implications

Our observations strongly support a complex crystal chemistry of the carbonates at extreme conditions. The experimentally determined crystallographic features, such as bond distances and C-O-C bond angle (Table 1 and Fig. 4) fully agree with computational studies (Oganov et al. 2008, 2013) which point out a limited flexibility of polymerized tetrahedral CO_4 units, yet with a very rich polymorphism. Furthermore, the presence of trivalent iron suggests that other compositions could be stabilized, in particular aluminium carbonates. Aluminium is the sixth most abundant element in the Earth's mantle (Anderson 1989). As yet, no anhydrous aluminium carbonates are known among mineral species under crustal conditions, however, at higher pressures, crystal chemistry can drastically change (Santoro et al. 2014; Zhang et al. 2014). Iron carbonates undergo red-ox reactions also at ambient pressure, but the iron phase normally formed is magnetite or its high pressure form (Boulard et al. 2011, 2012). The discovery of $Fe_{13}O_{19}$ in this experiment indicates that even the Fe-O system is considerably more complex than currently known. This is further confirmed with the recent reported discovery of a new iron oxide Fe_4O_5 (Lavina et al. 2011; Woodland et al. 2012; Guignard and Crichton 2014) whose composition is between magnetite Fe_3O_4 and wustite, FeO. It is then not surprisingly that at Mbar pressures other stoichiometries can also be stabilized. Although our experimental work reported here does not provide any information about the physical properties of these novel systems, the single-layer $Fe_{13}O_{19}$ structure, based on a pseudo-hexagonal iron network, may be related to unusual magnetic and electronic behavior. The observation of $Fe_{13}O_{19}$ may also indicate an instability of magnetite above the 100 GPa, perhaps with a similar mechanism as observed at much lower pressures (Woodland et al. 2012). Moreover, red-ox conditions are pressure-governed, and the results indicate a possible coexistence of diamond and reduced carbon, with carbonates and high Fe^{3+}/Fe^{2+}-bearing phases at Earth's core/mantle interface conditions. We finally observe that magnesite-rich carbonates are stabilized in chemical environments such as basalt subducting slabs. If carbonates in these rocks are stable down to the base of lower mantle, they very likely interact with iron-rich materials, and mixed-Fe/Mg carbonates may form, as well as significant elemental carbon as a result of iron-carbon red-ox coupling reactions. Diamonds may contribute to carbon recycling in upwelling plumes, differently to the denser carbonates and oxides (Fig. 5) that could sink to the base of lower mantle and participate further in deeper red-ox processes.

Acknowledgments

We acknowledge ESRF for provision of beamtime (experiment HS4720). MM acknowledges supports from the Deep Carbon Observatory (DCO).

References:

Anderson, D.L. (1989) Theory of the Earth. Blackwell Scientific Publications , Boston, MA.

Anderson, O.L. (1982) The Earth's core and the phase diagram of iron. Phil Trans R Soc Lond, A306, 21–35.

Arapan, S., De Almeida, J.S., and Ahuia, R. (2007) Formation of sp(3) hybridized bonds and stability of $CaCO_3$ at very high pressure. Physical Review Letters, 98, 268501.

Berg, G.W. (1986) Evidence for carbonate in the mantle. Nature, 324, 50-51.

Boulard, E., Gloter, A., Corgne, A., Antonangeli, D., Auzende, A.L., Perrillat, J.P., Guyot, F., and Fiquet, G. (2011) New host for carbon in the deep Earth. Proceedings of the National Academy of Sciences of the United States of America, 108, 5184-5187.

Boulard, E., Menguy, N., Auzende, A.L., Benzerara, K., Bureau, H., Antonangeli, D., Corgne, A., Morard, G., Siebert, J., Perrillat, J.P., Guyot, F., and Fiquet, G. (2012) Experimental investigation of the stability of Fe-rich carbonates in the lower mantle. Journal of Geophysical Research, 117, B02208.

Busing, W., and Levy, H.A. (1967) Angle Calculations for 3- and 4- Circle X-ray and Neutron Diffractometers. Acta Crystallographica, 22, 457-464.

Datchi, F., LeToullec, R., and Loubeyre, P. (1997) Improved calibration of the SrB_4O_7: Sm $^{2+}$ optical pressure gauge: Advantages at very high pressures and high temperatures. Journal of Applied Physics 81, 3333-3339.

Fei, Y., Ricolleau, A., Frank, M., Mibe, K., Shen, G., and Prakapenka, V. (2007) Toward an internally consistent pressure scale. Proceedings of the National Academy of Sciences of the United States of America, 104, 9182–9186.

Guignard, J., and Crichton, W.A. (2014) Synthesis and recovery of bulk Fe_4O_5 from magnetite, Fe_3O_4. A member of a self-similar series of structures for the lower mantle and transition zone. Mineralogical Magazine, 78, 361-371.

Isshiki, M., Irifune, T., Hirose, K., Ono, S., Ohishi, Y., Watanuki, T., Nishibori, E., Takata, M., and Sakata, M. (2004) Stability of magnesite and its high-pressure form in the lowermost mantle. Nature, 427, 60–63.

Knittle, E., and Jeanloz, R. (1991) Earth's core-mantle boundary: Results of experiments at high pressures and temperatures. Science, 251, 1438-1443.

Lavina, B., Dera, P., Downs, R.T., Yang, W., Sinogeikin, S., Meng, Y., Shen, G., and Schiferl, D. (2010). Structure of siderite $FeCO_3$ to 56 GPa and hysteresis of its spin-pairing transition. Physical Review B, 82, 064110.

Lavina, B., Dera, P., Kim, E., Meng, Y., Downs, R.T., Weck, P.F., Sutton. S.R., and Zhao, Y. (2011) Discovery of the recoverable high-pressure iron oxide Fe_4O_5. Proceedings of the National Academy of Sciences of the United States of America, 42, 17281-17285.

Merlini, M., and Hanfland, M. (2013) Single-crystal diffraction at megabar conditions by synchrotron radiation. High Pressure Research, 33, 511-522.

Merlini, M., Hanfland, M., Gemmi, M., Huotari, S., Simonelli, L., and Strobel, P. (2010) Fe^{3+} spin transition in $CaFe_2O_4$ at high pressure. American Mineralogist, 95, 200-203.

Oganov, A.R., Hemley, R.J., Hazen, R.M., and Jones, A.P. (2013) Structure, bonding, and mineralogy of carbon at extreme conditions. Reviews in Mineralogy and Geochemistry, 75, 47-77.

Oganov, A.R., Ono, S., Ma, Y.M., Glass C.W., and Garcia, A. (2008) Novel high-pressure structures of $MgCO_3$, $CaCO_3$ and CO_2 and their role in Earth's lower mantle. Earth and Planetary Science Letters, 273, 38-47.

Oszlányi, G., and Suto, A. (2010). Ab initio structure solution by charge flipping. Acta Crystallographica Section A: Foundations of Crystallography, 60, 134-141.

Otsuka, K., and Karato, S.I. (2012) Deep penetration of molten iron into the mantle caused by a morphological instability. Nature, 492, 243-246.

Oxford Diffraction (2008). Crysalis RED, Version 1.171.32.29.

Palatinus, L., and Chapuis, G. (2007) SUPERFLIP-a computer program for the solution of crystal structures by charge flipping in arbitrary dimensions. Journal of Applied Crystallography, 40, 786-790.

Petitgirard, S., Salamat, A., Beck, P., Weck, G., and Bouvier, P. (2014) Strategies for in situ laser heating in the diamond anvil cell at an X-ray diffraction beamline. Journal of Synchrotron Radiation, 21, 89-96.

Petříček, V., Dušek, M., and Palatinus, L. (2014) Crystallographic Computing System JANA2006: General features. Zeitschrift für Kristallographie-Crystalline Materials, 229, 345-352.

Pullar, R.C. (2012) Hexagonal ferrites: A review of the synthesis, properties and applications of hexaferrite ceramics. Progress in Materials Science, 57, 1191-1334.

Rohrbach, A., and Schmidt, M.W. (2011) Redox freezing and melting in the Earth’s deep mantle resulting from carbon–iron redox coupling. Nature, 472, 209–212.

Salamat, A., Fischer, R.A., Briggs, R., McMahon, M.I., and Petitgirard, S. (2014) In situ synchrotron X-ray diffraction in the laser-heated diamond anvil cell: Melting phenomena and synthesis of new materials. Coordination Chemistry Reviews, 277-278, 15-30.

Santoro, M., Gorelli, F.A., Bini, R., Salamat, A., Garbarino, G., Levelut, C., Cambon, O., and Haines, J. (2014) Carbon enters silica forming a cristobalite-type CO_2–SiO_2 solid solution. Nature communications, 5, 3761.

Shannon, R.D. (1976) Revised effective ionic-radii and systematic studies of interatomic distances in halides and chalcogenides. Acta Crystallographica A32, 751–767.

Tao, R., Fei, Y., and Zhang, L. (2013) Experimental determination of siderite stability at high pressure. American Mineralogist, 98, 1565-1572.

Wierzbicka-Wieczorek, M., Kolitsch, U., and Tillmans, E. (2010). $Ba_2Gd_2(Si_4O_{13})$: a silicate with finite Si_4O_{13} chains. Acta Crystallographica, C66, i29-i32.

Woodland, A.B., Frost, D.J., Trots, D.M., Klimm, K., and Mezouar, M. (2012) In situ observation of the breakdown of magnetite (Fe_3O_4) to Fe_4O_5 and hematite at high pressures and temperatures. American Mineralogist, 97, 1808-1811.

Zhang, L., Meng, Y., Yang, W., Wang, L., Mao, W.L., Zeng, Q.S., Jeong, J.S., Wagner, A.J., Mkhoyan, K.A., Liu, W., Xu, R., and Mao, H.K. (2014) Disproportionation of $(Mg,Fe)SiO_3$ perovskite in Earth's deep lower mantle. Science, 344, 877-882.

Figures and tables

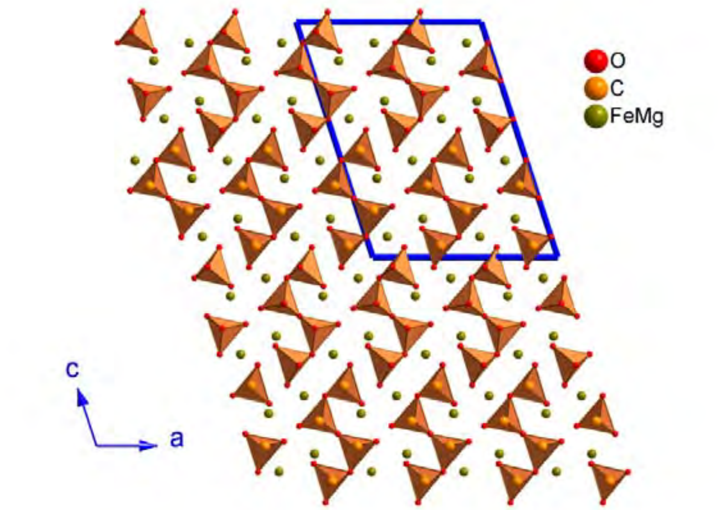

Fig. 1. Crystal structure of $Mg_2Fe_2(C_4O_{13})$, based on truncated tetrahedral carbonate chains.

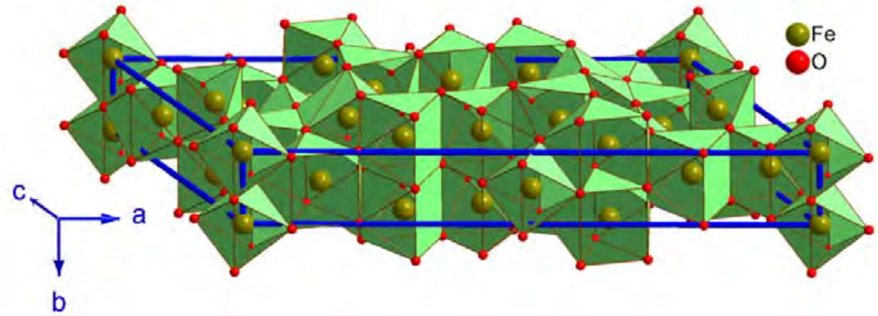

Fig. 2. Crystal structure of $Fe_{13}O_{19}$

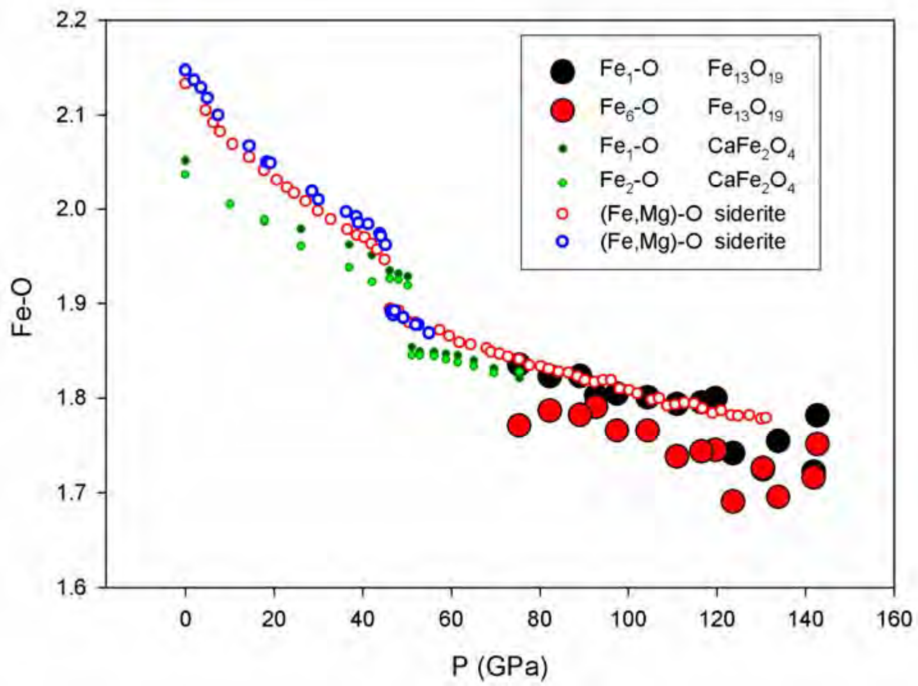

Fig. 3. – Interatomic Fe-O distances in octahedral sites in $Fe_{13}O_{19}$, and comparison with literature data for Fe^{3+}-O octahedral distances in $CaFe_2O_4$ (Merlini et al. 2010) and Fe^{2+}-O distances in siderite (blue empty circles: Lavina et al., 2010; red empty circles: Merlini et al. 2013).

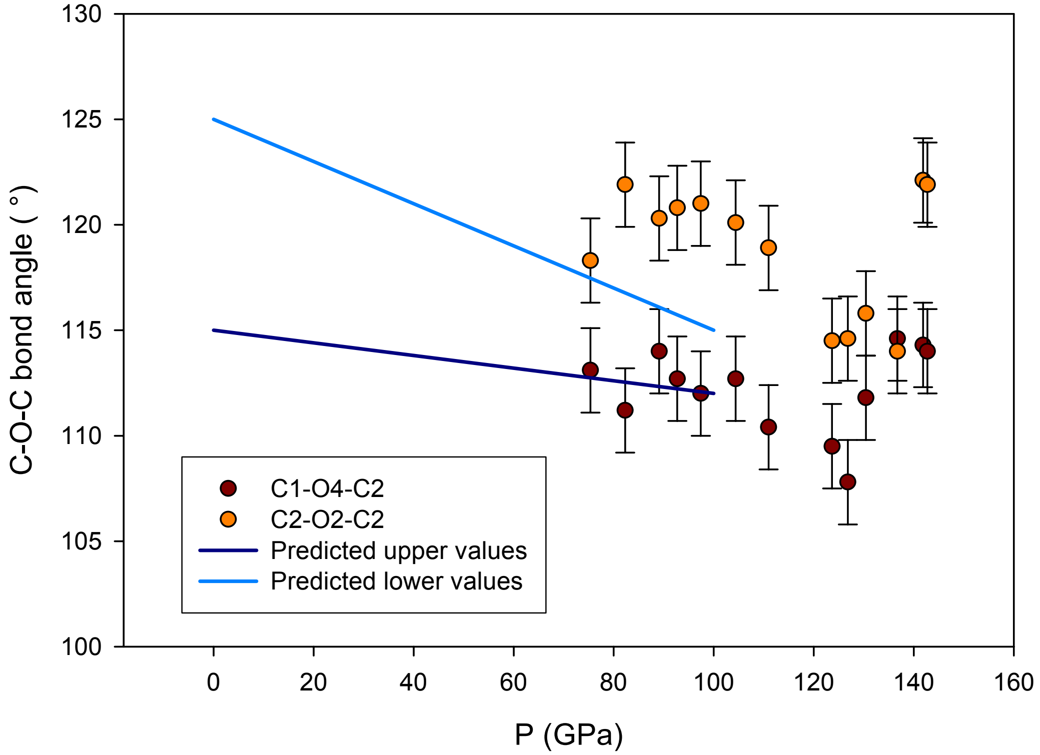

Fig. 4. - C-O-C bond angles determined at various pressures and comparison with predicted values (Oganov et al., 2008; Oganov et al., 2014). The experimental values are in close agreement with prediction, within experimental accuracy and chemical difference between $H_6C_2O_6$ used in computation and $Mg_2Fe_2(C_4O_{13})$.

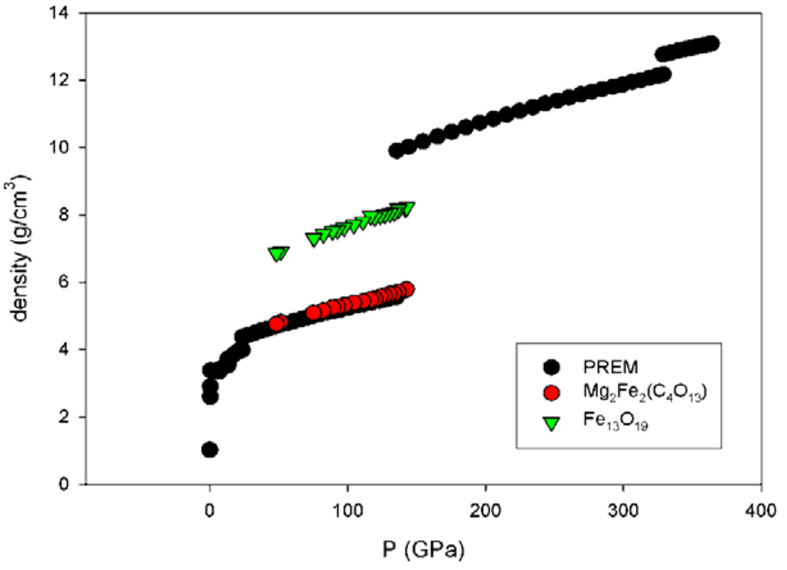

Fig. 5 – Density of $Mg_2Fe_2(C_3O_{13})$ and $Fe_{13}O_{19}$ as function of pressure, compared with PREM model

Atom	**x**	**y**	**z**	**U (Å ^{2})**	**Bond distances (Å) and angles (°)**	
(Mg,Fe)$_1$	0.8848(5)	-0.0245(9)	0.4113(3)	0.0237(13)	C_1-O_4	1.24(5)
(Mg,Fe)$_2$	0.6619(5)	-0.4841(9)	0.3355(3)	0.0186(13)	C_1-O_5	1.35(4)
O_1	0.808(2)	0.317(3)	0.2843(13)	0.020(4)	C_1-O_6	1.31(3)
O_2	0.5	-0.197(5)	0.25	0.024(6)	C_1-O_7	1.31(2)
O_3	0.9380(18)	0.798(3)	0.3018(12)	0.006(3)	C_2-O_1	1.18(3)
O_4	0.997(2)	-0.376(3)	0.5881(13)	0.013(3)	C_2-O_2	1.36(3)
O_5	0.8149(18)	-0.524(3)	0.6211(13)	0.013(3)	C_2-O_3	1.291(19)
O_6	0.813(2)	-0.424(3)	0.4581(15)	0.012(3)	C_2-O_4	1.51(3)
O_7	0.909(2)	-0.880(3)	0.5420(15)	0.021(4)		
C_1	0.889(3)	-0.552(5)	0.550(2)	0.015(5)	C_2-O_2-C_2	122.1(17)
C_2	1.084(2)	-0.472(4)	0.7012(18)	0.005(3)	C_1-O_4-C_2	114.3(19)

Table 1. Atomic coordinates, isotropic displacement parameters and selected interatomic distances and bonding angles for $Mg_2Fe_2(C_4O_{13})$, monoclinic, *C*2/*c*, a=9.822(3) b=3.9023(13) c= 13.154(5) Å β=108.02(3)° V=479.4(3) Å^3 at 135 GPa.

Atom	**x**	**y**	**z**	**U (Å ^{2})**	**Bond distances (Å)**	
Fe_1	0.4267(5)	-0.5	0.4606(5)	0.0128(11)	Fe_6-O_9 (x2)	1.68(3)
Fe_2	0.2641(4)	0	0.3647(4)	0.0110(10)	Fe_6-O_{10} (x4)	1.706(11)
Fe_3	0.4645(4)	-1	0.2289(5)	0.0134(11)	Fe_1-O_1 (x2)	1.814(6)
Fe_4	0.6273(4)	-1	0.3428(5)	0.0110(10)	Fe_1-O_2	1.76(2)
Fe_5	0.3501(4)	0	0.0691(4)	0.0120(10)	Fe_1-O_5	1.76(2)
Fe_6	0.5	-0.5	0	0.0181(16)	Fe_1-O_6 (x2)	1.66(2)
Fe_7	0.3142(4)	0	0.1576(5)	0.0107(10)		
O_1	0.5	0	0.5	0.022(8)		
O_2	0.4017(16)	-0.5	0.258(2)	0.017(5)		
O_3	0.3012(16)	0.5	0.5243(19)	0.006(4)		
O_4	0.1609(15)	0	0.2278(18)	0.007(4)		
O_5	0.4525(19)	-0.5	0.664(2)	0.026(5)		
O_6	0.367(2)	0	0.426(2)	0.018(5)		
O_7	0.3024(18)	-0.5	-0.003(2)	0.015(4)		
O_8	0.2469(13)	0	-0.2223(17)	0.000(4)		
O_9	0.5692(16)	-0.5	-0.059(2)	0.013(4)		
O_{10}	0.4566(17)	0	-0.130(2)	0.011(4)		

Table 2. Atomic coordinates, isotropic displacement parameters and Fe-O interatomic distances in octahedral sites for $Fe_{13}O_{19}$, monoclinic, *C*2/*m*, a=19.233(2) b=2.5820(13) c=9.550(11) Å β=118.39(3)° V=417.2(5) Å^3 at 135 GPa.